



# ELASTIC WAVE EMISSION DURING DELAMINATION GROWTH OF CARBON/EPOXY MONITORED WITH FIBER-OPTIC DEFEW STRAIN RATE SENSOR

Kazuro Kageyama\*, Hideaki Murayama\*, Sakura Atsuta\*,  
Isamu Ohsawa\* and Makoto Kanai\*

\* Department of Environmental and Ocean Engineering, The University of Tokyo

**Keywords:** CFRP, Delamination, DCB Test, Acoustic Emission, Fiber-optic Sensor

## Abstract

A fiber-optic sensor with very large bandwidth and extremely high sensitivity has been developed based on Doppler effect in flexible and expandable light waveguide (DEFEW). Fiber-optic DEFEW sensor is applied to detect elastic waveforms emitted during the delamination growth in DCB specimen. Principle, sensitivity of circular loop sensor configuration and setup of measuring system are briefly explained. Unidirectional carbon/epoxy systems of T800H/3631 (base line) and T800H/3900-2 (toughened) are used for the DCB tests. DCB tests are carried out, and AE waveforms are detected with a pair of upside and downside sensors. The fiber-optic sensors are flexible and they detect AE events inside the gauge length. The test results indicate that signs of the first arrival peak detected with upside and downside sensors have related to the failure mode of breakage of bridging fibers and matrix cracking,

## 1 Introduction

Delamination is one of the most critical fractures of composite materials. It is necessary to examine and improve the interlaminar fracture toughness for highly reliable use of composite materials, especially in case of being employed to primary structure.

Mode I interlaminar fracture toughness,  $G_{IC}$ , is measured by simulating the delamination process with the double cantilever beam test. Microscopic behavior during delamination is very complicated and more difficult to evaluate.

Monitoring of Acoustic emission (AE) is very appropriate tool to monitor microscopic failure events. AE is elastic waves caused by microscopic

failure. Generally PZT sensors are applied to AE monitoring [1]. They cannot be in use on curved surfaces so it is difficult to put them near AE sources in DCB specimens. Meanwhile a fiber-optic sensor has flexibility and it is possible to detect AE without damping of high-frequency component.

Authors have been developed a new fiber-optic strain rate sensor, which is based on Doppler effect in flexible and expandable light-waveguide (DEFEW) [2]. Fiber-optic DEFEW sensor has been applied to health monitoring of composite and concrete structures [3-5]. Fiber-optic DEFEW sensor has extremely high resolution less than nano-strain ( $10^{-10}$ ) in the very wide frequency range from 1 kHz to 1 MHz. In this study, transient strain rate signals in the DCB test were detected by the fiber-optic DEFEW strain rate sensors and analyzed in time and frequency domains to examine microscopic behavior during delamination.

## 2 Doppler effect in flexible and expandable light-waveguide (DEFEW)

### 2.1 Principle

Consider the light wave transmission in a media with refractive index,  $n$ . The light wave with frequency  $f_0$  emitted from a moving point A (light source) is detected at other moving point B (observer). The distance between points A and B changes from  $L$  to  $L+dL$  during infinitesimal time interval  $dt$ . Doppler frequency shift,  $f_D$ , is observed at B by the observer,

$$f_D = -\frac{n}{\lambda_0} \cdot \frac{dL}{dt} \quad (1)$$

,where  $\lambda_0$  is the light wavelength in a vacuum, and  $\lambda_0/n$  is the light wavelength in the media.

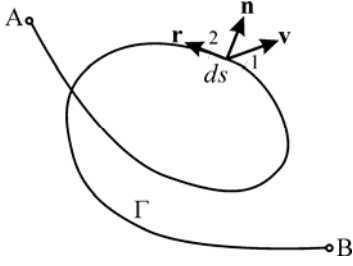


Fig. 1 Flexible and expandable light-waveguide.

Next, consider an arbitrary light path (light-waveguide),  $\Gamma$ , as shown in Fig. 1. The path is flexible and expandable. It has finite overall length,  $L$ , and two ends, denoted as points A and B, respectively. An incident light from the one end A (light source) is transmitted through the waveguide and detected at the other end B (observer). When the waveguide moves or vibrates, the same equation as Eq. (1) is applicable,

$$f_D = -\frac{n_{eq}}{\lambda_0} \cdot \frac{dL}{dt} \quad (2)$$

, where  $n_{eq}$  is the equivalent refractive index of the waveguide and  $\lambda_0/n_{eq}$  is the equivalent length of light wave in the waveguide.

From a geometrical consideration,  $dL/dt$  is given by Eq. (3),

$$\frac{dL}{dt} = [\mathbf{v} \cdot \mathbf{t}]_A^B + \int_{\Gamma} \kappa \cdot \mathbf{v} \cdot \mathbf{n} ds \quad (3)$$

, where  $\kappa$ ,  $\mathbf{v}$  and  $\mathbf{n}$  are the curvature, the velocity vector and the unit normal vector of the infinitesimal segment,  $ds$ , respectively, and  $\mathbf{t}$  is the unit direction vector defined at the end points A and B. (See Fig. 1.) The operation  $\bullet$  indicates inner product of two vectors. From Eqs. (2) and (3), we obtain the following equation;

$$f_D = -\frac{n_{eq}}{\lambda_0} [\mathbf{v} \cdot \mathbf{t}]_A^B - \frac{n_{eq}}{\lambda_0} \int_{\Gamma} \kappa \cdot \mathbf{v} \cdot \mathbf{n} ds \quad (4)$$

This equation implies ‘‘Doppler effect in flexible and expandable light-waveguide’’. Displacement rate normal to the small segment of bent optical fiber effects on the frequency shift of light transmitted through the optical fiber and that the intensity of the frequency shift is proportional to the curvature of the bent fiber. We can detect the local displacement rate at the bent region in the optical fiber. As a feature of sensors, output signal shall return to steady-state value when the external excitation is removed. It requests that the waveguide is elastic, or deformation is reversible.

## 2.2 Circular loop sensor

In the case of a circular loop sensor as shown in Fig. 2, the sensitivity of strain rate can be evaluated by integrating Eq. (4) on the strain rate field. For simplicity, the uniform strain rate field,  $\dot{\epsilon}_x$ ,  $\dot{\epsilon}_y$  and  $\dot{\gamma}_{xy}$  is assumed on the integration path. The velocity vector and unit normal vector are given by Eqs. (5) and (6), respectively, where polar coordinate system is employed as shown in Fig. 2.

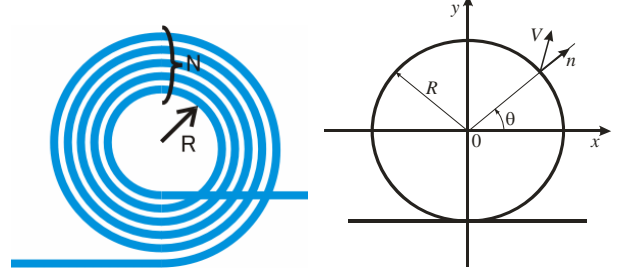


Fig. 2 Circular loop sensor

$$\mathbf{v} = R \left\{ \begin{array}{l} \dot{\epsilon}_x \cos \theta + \frac{1}{2} (\dot{\gamma}_{xy} + \dot{\omega}_{xy}) \sin \theta \\ \frac{1}{2} (\dot{\gamma}_{xy} - \dot{\omega}_{xy}) \cos \theta + \dot{\epsilon}_y \sin \theta \end{array} \right\} \quad (5)$$

$$\mathbf{n} = \left\{ \begin{array}{l} \cos \theta \\ \sin \theta \end{array} \right\} \quad (6)$$

, where  $\dot{\omega}_{xy}$  and  $R$  are rotation term of distortion and radius of the loop, respectively. Substituting Eqs. (5) and (6) into Eq. (4), the theoretical frequency shift,  $f_D^{th}$ , is obtained.

$$f_D^{th} = -\frac{\pi R n_{eq}}{\lambda_0} (\dot{\epsilon}_x + \dot{\epsilon}_y) = -\frac{\pi R n_{eq}}{\lambda_0} (\dot{\epsilon}_1 + \dot{\epsilon}_2) \quad (7)$$

The sum of the axial strain rates or the sum of the principal strain rates is converted into the Doppler frequency shift by applying circular loop sensor. Shear strain and rotation have no effect on the frequency shift. In the case of  $N$  turns of loop, as shown in Fig. 2 (left), the frequency shift becomes  $N$  times larger.

$$f_D^{th} = -\frac{N \pi R_{av} n_{eq}}{\lambda_0} (\dot{\epsilon}_x + \dot{\epsilon}_y) = -\frac{N \pi R_{av} n_{eq}}{\lambda_0} (\dot{\epsilon}_1 + \dot{\epsilon}_2) \quad (8)$$

, where  $R_{av} = (R_{max} + R_{min})/2$  is the average radius of the loop. The circular loop sensor has no directional sensitivity.

We can control the sensitivity of the sensor by changing the radius and number of turns. The size of the loop is equivalent to a gauge length of the sensor, and it is recommended that the gauge length should be sufficiently smaller than the wavelength of the elastic wave measured.

### 2.3 Setup of measurement system

A Laser Doppler velocimeter (LDV) as shown in Fig. 3 is used to detect the frequency shift. Detection electronics is FM discriminator. Light source is He-Ne laser (output power; 1mW, wavelength.  $\lambda_0$ : 632.8 nm), and heterodyne interference technique is applied to the measurement in the present paper. An acousto-optical modulator (AOM) changes the frequency of the reference light source from  $f_0$  to  $f_0+f_M$  ( $f_M = 80$  MHz) in order to produce beating signals with frequency of  $f_D+f_M$ .

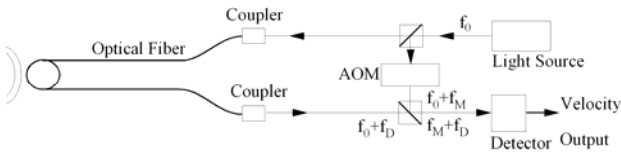


Fig. 3 Setup of measurement system.

The sensitivity of the optical circular loop sensor (average diameter: 20 mm, number of turn: 10) is calculated theoretically. By applying commercially available performance data of the LDV (Melectro, V1002) [6], the resolution and dynamic range were obtained and extremely high resolution less than nano-strain ( $10^{-10}$ ) is expected in the very wide frequency range from 1 kHz to 1 MHz. Low frequency vibration of 0.1 Hz is detectable with sufficient sensitivity. The resolution of the newly developed sensor is extremely superior to the other fiber optic sensors, such as FBG. The developed fiber-optic sensor covers the measurement range from conventional strain gauge to AE sensor.

### 3 Test Methods

#### 3.1 Specimen and Sensors

Unidirectional carbon/epoxy systems of T800H/3631 (baseline) and T800H/3900-2 (toughened) are used for the DCB tests (JIS K7086-1993/ISO15024-2001). The specimen is shown in Fig.4. The width, B, is 25mm, the overall length, L, is 175mm, and normal thickness, 2H, is 3mm. The initial crack was introduced by polyimide film with thickness of 13 $\mu$ m. The film was removed and a precrack was induced before the test.

Four fiber-optic sensors (average diameter, 20mm; number of turns of upside sensors, 20 /downside sensors, 20) and a PZT sensor were attached to the specimen. AE signals were detected

by two fiber-optic sensors (first, set A and next, set B) and a PZT sensor at the same time during the test.

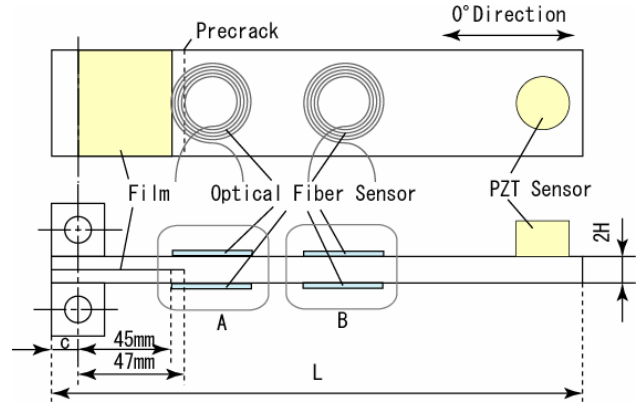


Fig.4 DCB specimen

#### 3.2 Test conditions

The cross head speed was controlled at 0.5mm/min during the DCB tests. Monotonic load was applied in order to detect AE signals continuously. AE signals were detected with the sampling rate 5MHz and the number of words of 5000. 10Hz high pass filter was used for signals derived from fiber-optic sensors. Crack length was measured using a traveling microscope.

#### 4 Detected AE waves

As shown in Fig.5, AE events started at the beginning of the crack growth. The total number of detected AE events during about 20 minutes' tests was around 2000.  $G_{IC}$  during crack propagation was nearly constant in the both case of T800H/3631 and T800H/3900-2.

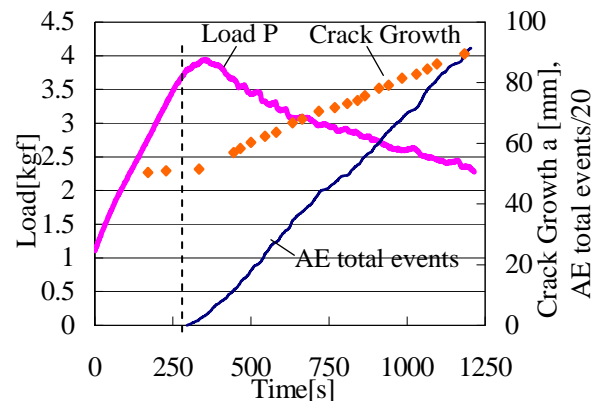
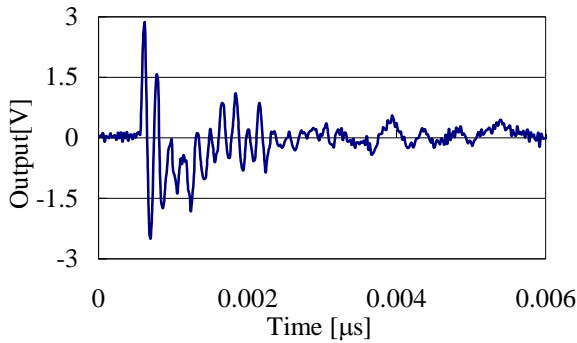


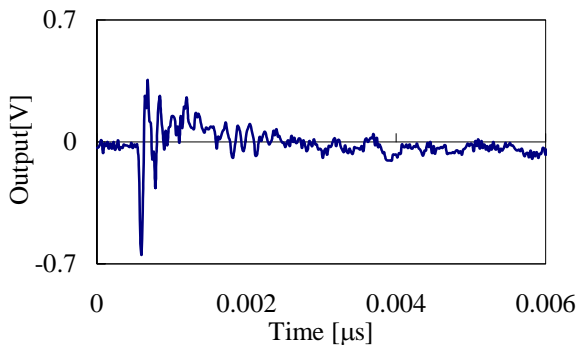
Fig.5 Relation of load, crack growth and AE events

Fig.6 shows an example of sets of AE signals detected by upside and downside fiber-optic DEFEW sensors at the same time. The waves show

clear inverse correlation. The AE source might be a release of dipole of forces, which is antisymmetric with respect to crack surface, though symmetric Mode I load is applied to the specimen..

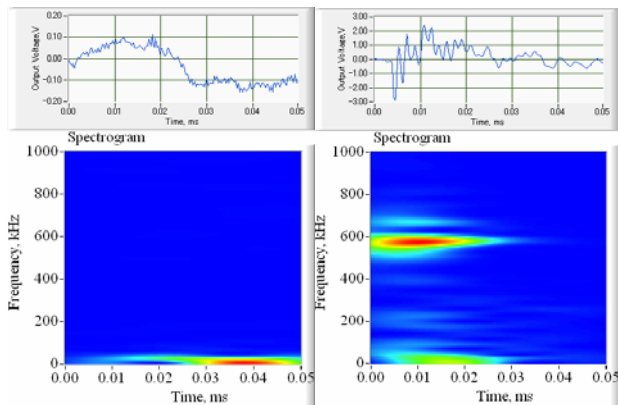


(a) Detected AE wave at upside surface



(b) Detected AE wave at downside surface

Fig.6 Example of comparison of AE signals between upside and downside fiber-optic sensors



(a) 20 kHz peak (b) 570 kHz peak  
Fig.7 Results of time-frequency analysis

In this experiment, several signals with different characteristics were detected. Two examples of the results of time-frequency analysis are given in Fig.7 (a) and (b) which show different frequency peak of 20kHz and 570kHz, respectively. These differences are considered of a result of different failures during delamination.

## 5 Discussions

### 5.1 Signs of first arrival peaks

Model specimens are prepared for breakage of bridging fiber (see Fig. 8) and for matrix cracking in adhesive layer between a pair of composite laminates. DCB tests of the model specimens are carried out, and the signs of first arrival peak detected with upside and downside sensors are examined.

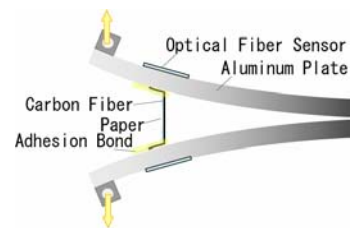


Fig. 8 Model specimen of bridging fiber

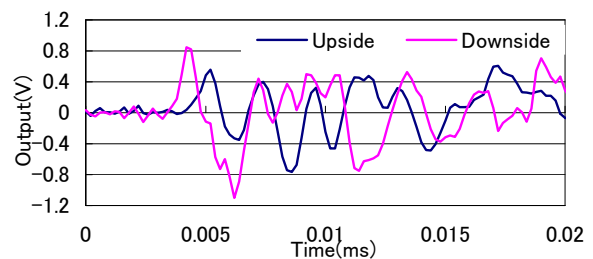


Fig. 9 Time history of elastic wave of breakage of bridging fiber

As shown in Fig. 9, signs of first arrival peak of breakage of bridging fiber are positive/positive (expansion/expansion), and it well explains the release of dipole forces normal to the crack surface. On the other hand, most of signs of first arrival peak at matrix cracking are positive/negative or negative/positive, and the AE sources might be a release of dipole of forces which is antisymmetric with respect to crack surface, or shear fracture.

Signs of first arrival peak of DCB tests of T800H/3631 (baseline) and T800H/3900-2 (toughened) specimens are listed in Table 1 compared with the results of the model specimens.

Table 1 Percentage of sign of first arrival peaks detected with upside and downside sensor

Sign	Baseline T800H/3631	Toughened T800H/3900-2	Matrix cracking	Fiber break
+/+	15	10	5	100
-/-	17	19	0.	0
+/-	30	40	67	0
-/+	38	31	28	0
		71	95	0

Around 70% of first arrival peaks of baseline and toughened carbon/epoxy systems show opposite signs, which suggest major failure mode is matrix cracking in the DCB test.

### 5.2 Histograms of AE parameters

AE parameters, such as time difference between first arriving peaks, maximum amplitude and half cycle of the first arriving peak, are categorized as signs of first arriving peak.

Histograms of time difference between first arriving peaks detected with upside and downside sensors are shown in Fig. 10. AE events with positive/positive signs have longer time difference between upside and downside sensors than those with opposite signs. AE events of fiber break occur at upper and lower ends of a bridging fiber, which result in difference of arrival time.

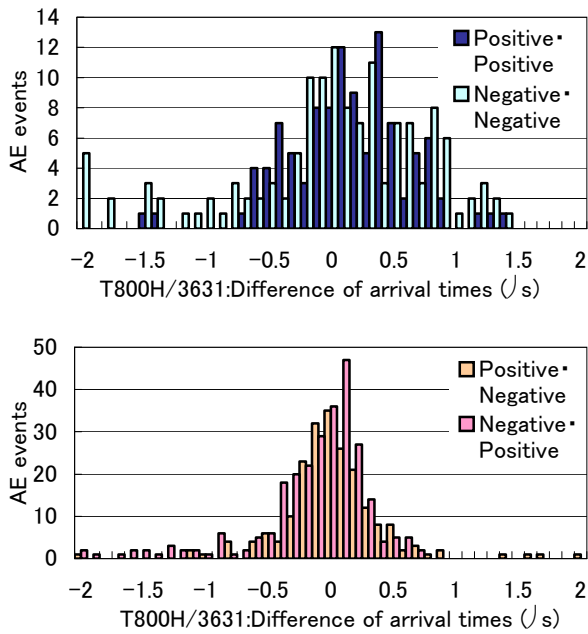


Fig. 10 Time difference between first arrival peaks detected with upside and downside sensor

Histograms of maximum amplitude of AE events of T800H/3631 (baseline) and T800H/3900-2 (toughened) are shown in Figs. 11 and 12, respectively. Average of peak amplitude of T800H/3631 is larger than that of T800H/3900-2 in positive/negative or negative/positive sign data group, which relates to matrix cracking. Histograms of positive/positive sign data group show small difference between T800H/3631 and T800H/3900-2, because they are reinforced with same reinforcement fiber.

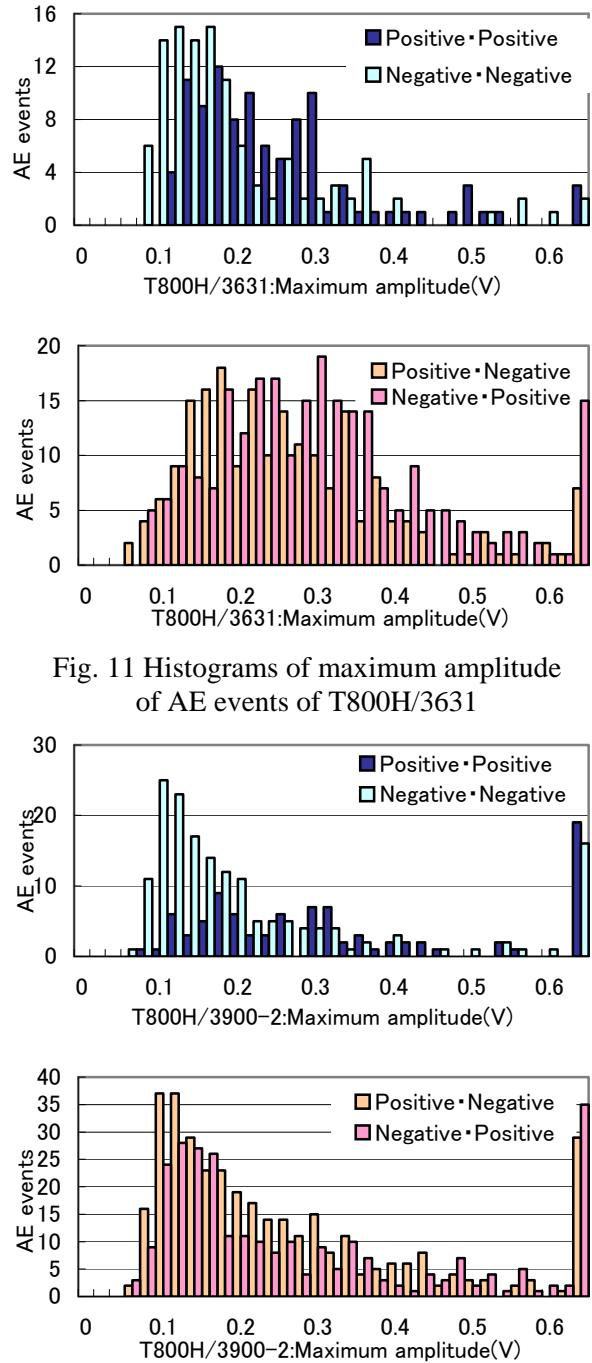


Fig. 11 Histograms of maximum amplitude of AE events of T800H/3631

Fig. 12 Histograms of maximum amplitude of AE events of T800H/3900-2

Half cycle of first arrival peak might relate to duration of failure process. Histograms of the half cycle,  $T_f$ , of opposite sign AE event group of T800H/3631 and T800H/3900-2 are shown in Fig. 13. Average time of T800H/3900-2 is longer than that of T800H/3631, and it suggests that failure process of T800H/3900-2 is more ductile than that of T800H/3631. Toughness of matrix system has

some effects on AE parameters detected with fiber-optic DEFEW sensor.

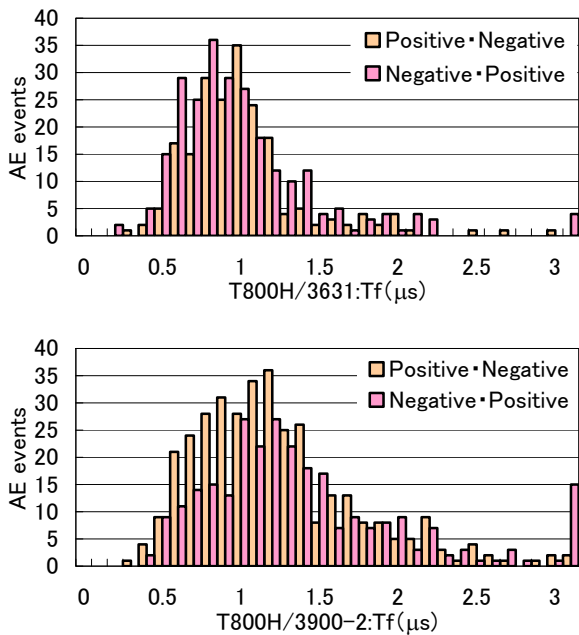


Fig. 13 Histograms of half cycle of first arrival peak

## 6 Conclusions

AE signals, which have physical meaning of strain rate, were detected by the fiber-optic DEFEW sensors during Mode I delamination tests. Fiber-optic DEFEW sensor has successfully applied to microscopic evaluation of failure process of composite materials.

The results suggest that failure of matrix resin occurs in shear mode under Mode I loading. First arrival peaks of AE events are analyzed and they are categorized four modes, and three of them might be related to breakage of bridging fibers and matrix cracking. Several different characteristics in time-frequency domain were also observed.

## 7 Acknowledgements

The authors thank Mr. Yuich Machijima, LAZOC, Inc. for technical supports to the new fiber-optic sensing system.

## References

- [1] I. Ndiaye, A. Maslouhi, and J. Denault "Characterization of Interfacial Properties of Composite Materials by Acoustic Emission". *Polymer Composites*, Vol.21, No.4 pp 595-604, 2000.
- [2] Kageyama K., Murayama H., Uzawa K., Ohsawa I., Kanai M, Akematsu Y., Nagata K., and Ogawa T.

"Doppler Effect in Flexible and Expandable Light Wave guide and Development of New Fiber-Optic Vibration/Acoustic Sensor". *Journal of Lightwave Technology*, Vol. 24, No. 4, pp 1768-1775, 2006.

- [3] K. Kageyama, H. Murayama, I. Ohsawa, M. Kanai, T. Motegi, K. Nagata, Y. Machijima and F. Matsumura, Development of a New Fiber-Optic Acoustic/Vibration Sensor: Principle, Sensor Performance, Applicability to Health Monitoring and Characteristics at Elevated Temperature, *Structural Health Monitoring 2003*, DEStech Publications, PA, pp.1150-1157, 2003.
- [4] K. Kageyama, H. Murayama, I. Ohsawa, M. Kanai, K. Nagata, Y. Machijima, F. Matsumura, Acoustic Emission Monitoring of a Reinforced Concrete Structure by Applying New Fiber-Optic Sensors, *Smart Materials and Structures*, Vol. 14, pp. S52-S59, 2005.
- [5] K. Kageyama, H. Murayama, I. Ohsawa, K. Uzawa, M. Kanai, Y. Akematsu and T. Matsuo, "Measurement of Failure Processes in Carbon/Epoxy Composite Laminates by using a Fiber-Optic Strain Rate Sensor", *Proceedings of the 5th International Conference on Structural Health Monitoring*, Stanford University, Stanford, CA, Sept. 12-14, 2005, pp.709-715.
- [6] Technical Report of "VIBRODUCER V1002", Denshigiken Co. Ltd., 2002.